Charge-discharge performance of $Na_{2/3}Fe_{1/3}Mn_{2/3}O_2$ positive electrode in an ionic liquid electrolyte at 90 ºC for sodium secondary batteries

Changsheng Ding [a], Toshiyuki Nohira [b,*], and Rika Hagiwara [a,*]

[a] Graduate School of Energy Science, Kyoto University, Sakyo-ku, Kyoto 606-8501, Japan

[b] Institute of Advanced Energy, Kyoto University, Uji 611-0011, Japan

* Corresponding authors: Tel.: +81 75 753 5822; fax: +81 75 753 5906.

E-mail addresses: nohira.toshiyuki.8r@kyoto-u.ac.jp (T. Nohira)

hagiwara@energy.kyoto-u.ac.jp (R. Hagiwara)

Abstract

Ionic liquid is a promising electrolyte for sodium secondary batteries because of its negligible volatility, low flammability, and high thermal and electrochemical stabilities. In this study, $Na_{2/3}Fe_{1/3}Mn_{2/3}O_2$ as a positive electrode material was synthesized by a solid-state reaction, and its charge-discharge performance was investigated at 90 °C in the ionic liquid electrolyte $Na[FSA]-[C_3C_1pyrr][FSA]$ (FSA = bis(fluorosulfonyl)amide; C_3C_1pyrr =

N-methyl-N-propylpyrrolidinium). The $Na_{2/3}Fe_{1/3}Mn_{2/3}O_2$ positive electrode delivered an initial discharge capacity of 227 mAh g^{-1} at a current rate of 20 mA g^{-1} in the voltage range of 2.0–4.3 V. This study is the first where the $Na_{2/3}Fe_{1/3}Mn_{2/3}O_2$ positive electrode demonstrated a high reversible discharge capacity, larger than 220 mAh g^{-1}, due to the high operation temperature in the ionic liquid electrolyte.

Keywords: Sodium secondary battery; $Na_{2/3}Fe_{1/3}Mn_{2/3}O_2$; Positive electrode; Ionic liquid electrolyte; Charge-discharge performance

1. Introduction

Sodium secondary batteries, as post lithium-ion batteries, are attracting much interest for large-scale energy storage because of the resource abundance, uniform distribution, and low cost of sodium compared to lithium [1-6]. In recent years, various positive electrode materials have been developed for room-temperature sodium secondary batteries, such as $Na_{0.44}MnO_2$ [7, 8], $NaCrO_2$ [9, 10], Na_xVO_2 [11], $NaCoO_2$ [12], $Na_2FeP_2O_7$ [13, 14], $Na_3V_2(PO_4)_3$ [15, 16], $Na_{2/3}Co_{2/3}Mn_{1/3}O_2$ [17, 18], $Na_xNi_{1/3}Mn_{2/3}O_2$ [19], $NaFeO_2$ [20], $Na_{2/3}Fe_{1/2}Mn_{1/2}O_2$ [4, 21, 22], $Na_{2/3}Fe_{2/3}Mn_{1/3}O_2$ [23] and $Na_{2/3}Fe_{1/3}Mn_{2/3}O_2$ [24]. Among these positive electrode materials, layered sodium transition metal oxides, $Na_{2/3}Fe_xMn_{1-x}O_2$, have attracted much attention as

promising positive electrodes because of elemental abundance, low cost, and high capacity.

Layered sodium transition metal oxides can be classified into two main groups according to

Delmas' classification [25]: P2-type and O3-type, in which the P and O refer to the sodium

ions accommodated at prismatic and octahedral oxygen sites, respectively, and the numbers

refer to the repeat period of the transition metal layer to Na layer. The P2-type materials

usually show high capacity. Yabuuchi et al. [4] investigated the electrochemical sodium

insertion reaction of a P2-type $Na_{2/3}Fe_{1/2}Mn_{1/2}O_2$ electrode, and showed that it delivered a

reversible capacity of 190 mAh g^{-1} in the voltage range of 1.5–4.3 V. Park et al. [22] studied a

P2-type chelating-agent-assisted $Na_{2/3}Fe_{1/2}Mn_{1/2}O_2$ material, and reported a reversible

capacity of 195 mAh g^{-1} in the voltage range of 1.5–4.2 V. Zhu et al. [26] prepared a

free-standing P2-$Na_{2/3}Fe_{1/2}Mn_{1/2}O_2$-graphene film that showed a reversible capacity of 156

mAh g^{-1} in the voltage range of 1.5–4.3 V with high Coulombic efficiency. Gonzalo et al. [23]

synthesized and investigated a P2-type $Na_{2/3}Fe_{2/3}Mn_{1/3}O_2$ positive electrode material and

showed that the reversible capacity was 151 mAh g^{-1} in the voltage range of 1.5–4.2 V. Zhao

et al. [24] investigated the electrochemical and thermal properties of P2-type

$Na_{2/3}Fe_{1/3}Mn_{2/3}O_2$, and reported an initial discharge capacity of 193 mAh g^{-1} in the range of

1.5–4.3 V.

Although $Na_{2/3}Fe_xMn_{1-x}O_2$ positive electrodes have shown high reversible capacities, there

are still some drawbacks: low rate capability and poor cycle performance. In addition, studies

on $Na_{2/3}Fe_xMn_{1-x}O_2$ were usually performed in organic electrolytes like $NaClO_4$/propylene carbonates (PC), which is disadvantageous for constructing large-scale safe batteries due to the high volatility and flammability of organic electrolytes. A safer alternative to organic electrolytes is needed. Ionic liquids have been considered promising candidates for sodium secondary batteries due to their low flammability, negligible volatility, and high thermal and electrochemical stabilities. $Na[FSA]$-$[C_3C_1pyrr][FSA]$ ionic liquids (FSA = bis(fluorosulfonyl)amide; C_3C_1pyrr = *N*-methyl-*N*-propylpyrrolidinium) were reported as promising electrolytes for sodium secondary batteries because they possess favorable properties in a wide temperature range [27, 28, 29]. Therefore, $Na[FSA]$-$[C_3C_1pyrr][FSA]$ ionic liquid was adopted as an electrolyte to investigate a $Na_{2/3}Fe_xMn_{1-x}O_2$ positive electrode in the present study. $Na_{2/3}Fe_{1/3}Mn_{2/3}O_2$ was synthesized by a solid-state reaction, and its charge-discharge performance was evaluated at 90 °C in the $Na[FSA]$-$[C_3C_1pyrr][FSA]$ ionic liquid. The $Na_{2/3}Fe_{1/3}Mn_{2/3}O_2$ positive electrode delivered a high discharge capacity of 227 mAh g^{-1} at a current rate of 20 mA g^{-1} in the voltage range of 2.0–4.3 V.

2. Experimental

$Na_{2/3}Fe_{1/3}Mn_{2/3}O_2$ powders were synthesized by a conventional solid-state reaction [4]. The starting materials, Na_2CO_3 (Sigma-Aldrich, 99.95%), α-Fe_2O_3 (Wako Pure Chemical

Industries, 99.9%), and Mn_2O_3 (Strem Chemicals, 99%), were mixed in stoichiometric proportions and were pressed into pellets. Then, the pellets were heated in air at 900 °C for 12 h. Finally, the pellets were ground to obtain $Na_{2/3}Fe_{1/3}Mn_{2/3}O_2$ powders. The dried $Na_{2/3}Fe_{1/3}Mn_{2/3}O_2$ powders were stored in an Ar-filled glove box

The crystalline phase of the synthesized powders was characterized via powder X-ray diffraction (XRD, Rigaku, SmartLab) using Cu-Kα radiation. The particle morphologies of the synthesized powders were observed using field-emission scanning electron microscopy (FE-SEM, Hitachi, SU8020).

$Na_{2/3}Fe_{1/3}Mn_{2/3}O_2$ positive electrodes were prepared by completely mixing the $Na_{2/3}Fe_{1/3}Mn_{2/3}O_2$ powders with acetylene black (Wako Pure Chemical Industries) and polytetrafluoroethylene (Sigma-Aldrich) at a weight ratio of 80:15:5, using a mortar and pestle to obtain a thin film. The thin film was then pressed onto aluminum mesh current collectors and were used as positive electrodes. Metallic sodium discs (Sigma-Aldrich, purity >99.85%) were pressed on aluminum disc current collectors and were used as counter electrodes. Na[FSA]-[C_3C_1pyrr][FSA] ionic liquid was prepared by mixing Na[FSA] (Mitsubishi Materials Electronic Chemicals, purity >99.0%) and [C_3C_1pyrr][FSA] (Kanto Chemical Co., purity >99.9%) in a molar ratio of 2:8, and was used as an electrolyte. A glass fiber filter (Whatman, GF-A, 260 mm) was used as a separator. The $Na_{2/3}Fe_{1/3}Mn_{2/3}O_2$ positive electrode and the separators were vacuum-impregnated with the

Na[FSA]-[C$_3$C$_1$pyrr][FSA] ionic liquid at 60 °C before assembling the cells. Then, Na$_{2/3}$Fe$_{1/3}$Mn$_{2/3}$O$_2$/Na[FSA]-[C$_3$C$_1$pyrr][FSA]/Na half-cells were assembled using CR2032-type coin cells in an Ar-filled glove box.

Charge-discharge tests were conducted at constant current rates of 20-1000 mA g^{-1} in the voltage range of 1.5-4.3 V. The cycle performance was evaluated at constant current rates of 20, 100, 200, and 500 mA g^{-1}. All electrochemical measurements were performed at 90 °C. To investigate the crystalline phase of the Na$_{2/3}$Fe$_{1/3}$Mn$_{2/3}$O$_2$ positive electrodes at different charge-discharge states, ex-situ XRD analysis was performed. The Na$_{2/3}$Fe$_{1/3}$Mn$_{2/3}$O$_2$ electrodes were removed from the coin cells in an Ar-filled glove box, and were washed with anhydrous tetrahydrofuran (THF, Wako Pure Chemicals) to remove the electrolyte. The Na$_{2/3}$Fe$_{1/3}$Mn$_{2/3}$O$_2$ electrode was then placed in an air-tight sample holder for XRD analysis.

3. Results and discussion

The XRD pattern of the synthesized Na$_{2/3}$Fe$_{1/3}$Mn$_{2/3}$O$_2$ powders is shown in Fig. 1a, which shows the formation of a single phase. The diffraction peaks are indexed to a hexagonal lattice with space group $P6_3/mmc$, which is characteristic of P2-type layered structures [4]. The calculated lattice parameters were a = 0.2898 nm and c = 1.121 nm, which are close to reported values (a = 0.2913 nm and c = 1.127 nm) [24]. The diffraction peaks are also in

agreement with that of P2-$Na_{2/3}Fe_{1/3}Mn_{2/3}O_2$ powders reported in literature [24]. The SEM

image shown in Fig. 1b reveals that the particle size of the synthesized $Na_{2/3}Fe_{1/3}Mn_{2/3}O_2$

powders is in the range of 0.5–1 μm. In addition, some particles agglomerated, forming

secondary particles a few micrometers in diameter.

Fig. 2a shows the charge-discharge curves of the $Na_{2/3}Fe_{1/3}Mn_{2/3}O_2$ positive electrode at a

current rate of 20 mA g^{-1} in the voltage range of 1.5–4.2 V. In the first cycle, the charge

capacity is 116 mAh g^{-1}, which corresponds to the extraction of ~0.45 Na^+ ions from the

structure. The discharge capacity is 317 mAh g^{-1}, indicating an increase of sodium insertion

into the structure. However, the theoretical capacity based on a single-electron redox process

of an Me^{3+}/Me^{4+} (Me = $Fe_{1/3}Mn_{2/3}$) couple is 261 mAh g^{-1}, which indicates that some side

reactions occur during the first discharge process. Figure 2a shows a voltage plateau at 1.6 V,

which disappears gradually in subsequent charge-discharge cycles. Thus, the extra discharge

capacity may be attributed to the side reactions occurring at 1.6 V, which may be explained

by reactions of acetylene black with the ionic liquid as shown in Fig. S1. Although the

charge-discharge of $Na_{2/3}Fe_xMn_{1-x}O_2$ positive electrode in organic electrolytes is generally

conducted in the voltage range of 1.5–4.3 V [4, 21-24], the same voltage range is not suitable

for the present ionic liquid electrolyte. Thus, the lower cut-off voltage was changed to 2.0 V.

Fig. 2b shows the charge-discharge curves of the $Na_{2/3}Fe_{1/3}Mn_{2/3}O_2$ positive electrode in the

voltage range of 2.0–4.2 V. This condition suggests a reversible electrochemical intercalation

of sodium ions. The first discharge capacity is 204 mAh g^{-1}, which corresponds to the insertion of 0.78 Na^+ ions into the structure. The discharge capacity slightly decreases in subsequent cycles. The cycle performance in 2.0–4.2 V is better than that in 1.5–4.2 V; the coulombic efficiency reaches 99% in the second cycle.

The effect of cut-off voltage on discharge capacity is shown in Fig. 3. The discharge capacity decreases with a reduction in the cut-off voltage range. As described above, in the 1.5–4.2 V range, the discharge capacity is higher than the theoretical capacity of 261 mAh g^{-1}. When the lower cut-off voltages were raised to 2.0 V and 2.1 V (cut-off voltages: 2.0–4.2 V and 2.1–4.2 V, respectively), the discharge capacities decreased to 204 and 178 mAh g^{-1}, respectively. Furthermore, when the higher cut-off voltage was lowered to 4.0 V (cut-off voltage: 2.0–4.0 V), the first discharge capacity further declined to 165 mAh g^{-1}, but the discharge capacity increased slightly with increasing cycle number. However, when the upper cut-off voltage was raised to 4.3 V (cut-off voltage: 2.0–4.3 V), the discharge capacity increased to 227 mAh g^{-1}, which corresponds to 87% of the theoretical capacity. Thus, the cut-off voltage range strongly affects the discharge capacity of the $Na_{2/3}Fe_{1/3}Mn_{2/3}O_2$ positive electrode.

The observed initial discharge capacity of 227 mAh g^{-1} in the voltage range of 2.0–4.3 V is higher than those reported in organic electrolytes: 191 mAh g^{-1} for the $Na_{2/3}Fe_{1/3}Mn_{2/3}O_2$ electrode [24], 190–197 mAh g^{-1} for the $Na_{2/3}Fe_{1/2}Mn_{1/2}O_2$ electrodes [4, 21], 151 mAh g^{-1} for

the $Na_{2/3}Fe_{2/3}Mn_{1/3}O_2$ electrode [23], and 160 mAh g^{-1} for the $Na_{1/2}Fe_{1/2}Mn_{1/2}O_2$ electrode [30]. The high discharge capacity in an ionic liquid electrolyte is attributed to the high operation temperature. At lower temperatures, as shown in Fig. S2, the $Na_{2/3}Fe_{1/3}Mn_{2/3}O_2$ positive electrode exhibits lower capacities (144 mAh g^{-1} at 50 °C and 74 mAh g^{-1} at 25 °C), which is attributed to the higher viscosity and lower ionic conductivity of ionic liquid at lower temperatures [27]. To the best of our knowledge, this is the first study to show a discharge capacity larger than 220 mAh g^{-1} for a $Na_{2/3}Fe_xMn_{1-x}O_2$ positive electrode.

To investigate the change in crystal structure during the charge-discharge cycle, ex-situ XRD measurements for the $Na_{2/3}Fe_{1/3}Mn_{2/3}O_2$ positive electrode were performed at different charge-discharge states. Fig. 4 displays the ex-situ XRD patterns of the $Na_{2/3}Fe_{1/3}Mn_{2/3}O_2$ positive electrode obtained during the charge-discharge process. With charge to 4.2 V, the $Na_{2/3}Fe_{1/3}Mn_{2/3}O_2$ crystal phase is converted into an amorphous phase due to the extraction of ~0.45 Na^+ ions from the crystal lattice (Fig. 4 state-2). When the electrode is discharged to 2.0 V, the crystal phase appears again (Fig. 4 state-3). However, there are changes in the XRD pattern at state-3 as compared to state-1. The diffraction peaks at 16°, 32°, and 36° shift toward higher angles and the diffraction peaks at 39° and 43° shift slightly toward lower angles. According to the capacity, 0.78 Na^+ ions are inserted into the structure during the discharge process. Therefore, there are more than 2/3 Na^+ ions in the state-3, and insertion of the extra Na^+ ions results in the change of the crystal lattice   (a = 0.2898 nm and c = 1.121

nm) with a increasing to $a = 0.2962$ nm and c decreasing to $c = 1.103$ nm. When the

electrode is re-charged to 4.2 V, a similar phenomenon is observed (state-2 and state-4). Thus,

the Na^+ ion extraction and insertion was demonstrated to proceed reversibly in the

$Na_{2/3}Fe_{1/3}Mn_{2/3}O_2$ positive electrode.

Fig. 5 shows the rate capability of the $Na_{2/3}Fe_{1/3}Mn_{2/3}O_2$ positive electrode. The discharge

capacity decreases with increasing current rate. At 500 mA g^{-1}, the discharge capacity is 65

mAh g^{-1}, and 32% of the discharge capacity at 20 mA g^{-1} is retained. Except for the initial few

cycles, the coulombic efficiencies are higher than 99%. The $Na_{2/3}Fe_{1/3}Mn_{2/3}O_2$ positive

electrode has limited rate capability, as reported for $Na_{2/3}Fe_{1/2}Mn_{1/2}O_2$ positive electrodes [4,

22]. In addition, the discharge capacity decreases gradually with increasing cycle number at

current rates below 200 mA g^{-1}. This indicates that some capacity fading occurs at low current

rates. The capacity fading is attributed to some phase transformation (degradation of crystal

structure) occurring at high potential, which can be prevented by lowering the upper cut-off

voltage as shown in Fig. 3. Carbon coating the surface of $Na_{2/3}Fe_{1/3}Mn_{2/3}O_2$ powders is

expected to improve the rate capability [22].

Finally, the cycle performance of the $Na_{2/3}Fe_{1/3}Mn_{2/3}O_2$ positive electrode is shown in Fig. 6.

At 20 mA g^{-1}, the discharge capacity decreases from 209 mAh g^{-1} to 52 mAh g^{-1} before 50

cycles. This capacity loss is very large at low current rates. Cycle performance is notably

improved with increasing current rate. At 100, 200, and 500 mA g^{-1}, the capacity retentions

after 200 cycles are 28%, 46%, and 64%, respectively. The $Na_{2/3}Fe_{1/3}Mn_{2/3}O_2$ positive electrode exhibits better cycle performance at higher current rates. Thus, the capacity fading is shown to depend on both cycle number and current rate. In addition, the $Na_{2/3}Fe_{1/3}Mn_{2/3}O_2$ positive electrode shows 141 mAh g^{-1} discharge capacity in the first cycle and 123 mAh g^{-1} after 25 cycles at 500 mA g^{-1}. The latter value is higher than the value of ~60 mAh g^{-1} at 500 mA g^{-1}, shown in Fig. 5. This also indicates that the low current rate strongly affects the capacity fading of the $Na_{2/3}Fe_{1/3}Mn_{2/3}O_2$ positive electrode. Therefore, for practical usage of $Na_{2/3}Fe_{1/3}Mn_{2/3}O_2$ positive electrodes, more efforts are needed to improve their low rate capability and poor cycle performance, e.g. synthesizing nano-sized $Na_{2/3}Fe_{1/3}Mn_{2/3}O_2$ particles, doping other transition metals, and building conductive network-like carbon coating.

4. Conclusion

$Na_{2/3}Fe_{1/3}Mn_{2/3}O_2$ powder was synthesized by a solid-state reaction, and its charge-discharge performance was evaluated at 90 °C in a $Na[FSA]$-$[C_3C_1pyrr][FSA]$ ionic liquid electrolyte. The $Na_{2/3}Fe_{1/3}Mn_{2/3}O_2$ positive electrode showed a high discharge capacity of 227 mAh g^{-1} at a current rate of 20 mA g^{-1} in the voltage range of 2.0–4.3 V. However, the electrode showed limited cycle performance at a low current rate of 20 mA g^{-1}. The cycle

performance was improved by applying higher current rates like 500 mA g^{-1}. Although this study demonstrated the high capacity of $Na_{2/3}Fe_{1/3}Mn_{2/3}O_2$ as a positive electrode material, continued efforts are needed to improve its rate capability and cycle performance.

References

[1] B.L. Ellis, L.F. Nazar, Sodium and sodium-ion energy storage batteries, Curr. Opin. Solid State Mater. Sci. 16 (2012) 168-177.

[2] N. Yabuuchi, K. Kubota, M. Dahbi, S. Komaba, Research development on sodium-ion batteries, Chem. Rev. 114 (2014) 11636-11682.

[3] M.D. Slater, D. Kim, E. Lee, C.S. Johnson, Sodium-ion batteries, Adv. Funct. Mater. 23 (2013) 947-958.

[4] N. Yabuuchi, M. Kajiyama, J. Iwatate, H. Nishikawa, S. Hitomi, R. Okuyama, R. Usui, Y. Yamada, S. Komaba, P2-type $Na_x[Fe_{1/2}Mn_{1/2}]O_2$ made from earth-abundant elements for rechargeable Na batteries, Nat. Mater. 11 (2012) 512-517.

[5] L.P. Wang, L.H. Yu, X. Wang, M. Srinivasan, Z.C.J. Xu, Recent developments in electrode materials for sodium-ion batteries, J. Mater. Chem. A 3 (2015) 9353-9378.

[6] D. Kundu, E. Talaie, V. Duffort, L.F. Nazar, The emerging chemistry of sodium ion batteries for electrochemical energy storage, Angew. Chem. Int. Ed. 54 (2015) 3431-3448.

[7] E. Hosono, T. Saito, J. Hoshino, M. Okubo, Y. Saito, D. Nishio-Hamane, T. Kudo, H.S. Zhou, High power Na-ion rechargeable battery with single-crystalline $Na_{0.44}MnO_2$ nanowire electrode, J. Power Sources 217 (2012) 43-46.

[8] Y.L. Cao, L.F. Xiao, W. Wang, D.W. Choi, Z.M. Nie, J.G. Yu, L.V. Saraf, Z.G. Yang, J. Liu, Reversible sodium ion insertion in single crystalline manganese oxide nanowires with long cycle life, Adv. Mater. 23 (2011) 3155-3160.

[9] S. Komaba, C. Takei, T. Nakayama, A. Ogata, N. Yabuuchi, Electrochemical intercalation activity of layered $NaCrO_2$ vs. $LiCrO_2$, Electrochem. Commun. 12 (2010) 355-358.

[10] C.Y. Chen, K. Matsumoto, T. Nohira, R. Hagiwara, A. Fukunaga, S. Sakai, K. Nitta, S. Inazawa, Electrochemical and structural investigation of $NaCrO_2$ as a positive electrode for sodium secondary battery using inorganic ionic liquid NaFSA-KFSA, J. Power Sources 237 (2013) 52-57.

[11] M. Guignard, C. Didier, J. Darriet, P. Bordet, E. Elkaim, C. Delmas, P2-Na_xVO_2 system as electrodes for batteries and electron-correlated materials, Nat. Mater. 12 (2013) 74-80.

[12] T. Shibata, Y. Fukuzumi, W. Kobayashi, Y. Moritomo, Fast discharge process of layered cobalt oxides due to high Na^+ diffusion, Sci. Rep. 5 (2015) 9006.

[13] H. Kim, R.A. Shakoor, C. Park, S.Y. Lim, J.S. Kim, Y.N. Jo, W. Cho, K. Miyasaka, R. Kahraman, Y. Jung, J.W. Choi, $Na_2FeP_2O_7$ as a promising iron-based pyrophosphate cathode for sodium rechargeable batteries: a combined experimental and theoretical study, Adv. Funct. Mater. 23 (2013) 1147-1155.

[14] P. Barpanda, G.D. Liu, C.D. Ling, M. Tamaru, M. Avdeev, S.C. Chung, Y. Yamada, A. Yamada, $Na_2FeP_2O_7$: a safe cathode for rechargeable sodium-ion batteries, Chem. Mater. 25 (2013) 3480-3487.

[15] S. Li, Y.F. Dong, L. Xu, X. Xu, L. He, L.Q. Mai, Effect of carbon matrix dimensions on the electrochemical properties of $Na_3V_2(PO_4)_3$ nanograins for high-performance symmetric sodium-ion batteries, Adv. Mater. 26 (2014) 3545-3553.

[16] Z.L. Jian, L. Zhao, H.L. Pan, Y.S. Hu, H. Li, W. Chen, L.Q. Chen, Carbon coated $Na_3V_2(PO_4)_3$ as novel electrode material for sodium ion batteries, Electrochem. Commun. 14 (2012) 86-89.

[17] D. Carlier, J.H. Cheng, R. Berthelot, M. Guignard, M. Yoncheva, R. Stoyanova, B.J. Hwang, C. Delmas, The P2-$Na_{2/3}Co_{2/3}Mn_{1/3}O_2$ phase: structure, physical properties and

electrochemical behavior as positive electrode in sodium battery, Dalton Trans. 40 (2011) 9306-9312.

[18] J.H. Cheng, C.J. Pan, J.F. Lee, J.M. Chen, M. Guignard, C. Delmas, D. Carlier, B.J. Hwang, Simultaneous reduction of Co^{3+} and Mn^{4+} in P2-$Na_{2/3}Co_{2/3}Mn_{1/3}O_2$ as evidenced by X-ray absorption spectroscopy during electrochemical sodium intercalation, Chem. Mater. 26 (2014) 1219-1225.

[19] D.H. Lee, J. Xu, Y.S. Meng, An advanced cathode for Na-ion batteries with high rate and excellent structural stability, Phys. Chem. Chem. Phys. 15 (2013) 3304-3312.

[20] J. Zhao, L.W. Zhao, N. Dimov, S. Okada, T. Nishida, Electrochemical and thermal properties of alpha-$NaFeO_2$ cathode for Na-ion batteries, J. Electrochem. Soc. 160 (2013) A3077-A3081.

[21] G. Singh, B. Acebedo, M.C. Cabanas, D. Shanmukaraj, M. Armand, T. Rojo, An approach to overcome first cycle irreversible capacity in P2-$Na_{2/3}[Fe_{1/2}Mn_{1/2}]O_2$, Electrochem. Commun. 37 (2013) 61-63.

[22] K. Park, D. Han, H. Kim, W.S. Chang, B. Choi, B. Anass, S. Lee, Characterization of a P2-type chelating-agent-assisted $Na_{2/3}Fe_{1/2}Mn_{1/2}O_2$ cathode material for sodium-ion batteries, RSC Adv. 4 (2014) 22798-22802.

[23] E. Gonzalo, M.H. Han, J.M.L. del Amo, B. Acebedo, M. Casas-Cabanas, T. Rojo, Synthesis and characterization of pure P2- and O3-$Na_{2/3}Fe_{2/3}Mn_{1/3}O_2$ as cathode materials for

Na ion batteries, J. Mater. Chem. A 2 (2014) 18523-18530.

[24] J. Zhao, J. Xu, D.H. Lee, N. Dimov, Y.S. Meng, S. Okada, Electrochemical and thermal properties of P2-type $Na_{2/3}Fe_{1/3}Mn_{2/3}O_2$ for Na-ion batteries, J. Power Sources 264 (2014) 235-239.

[25] C. Delmas , C. Fouassier, P. Hagenmuller, Structural classification and properties of the layered oxides, Physica B+C 99 (1980) 81-85.

[26] H.L. Zhu, K.T. Lee, G.T. Hitz, X.G. Han, Y.Y. Li, J.Y. Wan, S. Lacey, A.V. Cresce, K. Xu, E. Wachsman, L.B. Hu, Free-standing $Na_{2/3}Fe_{1/2}Mn_{1/2}O_2$@graphene film for a sodium-ion battery cathode, ACS Appl. Mater. Interfaces, 6 (2014) 4242-4247.

[27] C. Ding, T. Nohira, R. Hagiwara, K. Matsumoto, Y. Okamoto, A. Fukunaga, S. Sakai, K. Nitta, S. Inazawa, Na[FSA]-[C_3C_1pyrr][FSA] ionic liquids as electrolytes for sodium secondary batteries: Effects of Na ion concentration and operation temperature, J. Power Sources 269 (2014) 124-128.

[28] C.S. Ding, T. Nohira, K. Kuroda, R. Hagiwara, A. Fukunaga, S. Sakai, K. Nitta, S. Inazawa, NaFSA-C_1C_3pyrFSA ionic liquids for sodium secondary battery operating over a wide temperature range, J. Power Sources 238 (2013) 296-300.

[29] K. Matsumoto, Y. Okamoto, T. Nohira, R. Hagiwara, Thermal and transport properties of Na[N(SO_2F)$_2$]–[N-Methyl-N-propylpyrrolidinium][N(SO_2F)$_2$] ionic liquids for Na secondary batteries, J. Phys. Chem. C 119 (2015) 7648-7655.

[30] J.S. Thorne, R.A. Dunlap, M.N. Obrovac, Structure and electrochemistry of

$Na_xFe_xMn_{1-x}O_2$ (1.0 <= x <= 0.5) for Na-ion battery positive electrodes, J. Electrochem. Soc.

160 (2013) A361-A367.

Figure Captions

Figure 1. (a) XRD pattern and (b) SEM image of the synthesized $Na_{2/3}Fe_{1/3}Mn_{2/3}O_2$ powders.

Figure 2. Charge-discharge curves of the $Na_{2/3}Fe_{1/3}Mn_{2/3}O_2$ positive electrode at a current rate

of 20 mA g^{-1} and cut-off voltages of (a) 1.5–4.2 V and (b) 2.0–4.2 V.

Figure 3. Discharge capacity of the $Na_{2/3}Fe_{1/3}Mn_{2/3}O_2$ positive electrode at different cut-off

voltages for current rate of 20 mA g^{-1}.

Figure 4. XRD patterns of the $Na_{2/3}Fe_{1/3}Mn_{2/3}O_2$ positive electrodes at different

charge-discharge states: (1) before cycle; (2) charge to 4.2 V; (3) discharge to 2.0 V; and (4)

recharge to 4.2 V.

Figure 5. Rate capability of the $Na_{2/3}Fe_{1/3}Mn_{2/3}O_2$ positive electrode in the voltage range of

2.0–4.2 V.

Figure 6. Cycle performance of the $Na_{2/3}Fe_{1/3}Mn_{2/3}O_2$ positive electrode at current rates of
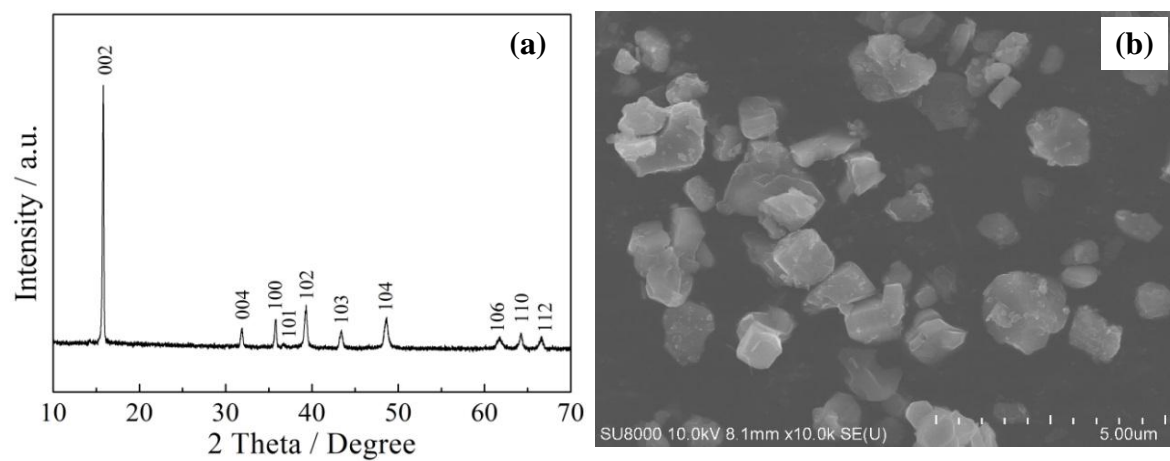
20–500 mA g^{-1} in the voltage range of 2.0–4.2 V.

Figure 1. (a) XRD pattern and (b) SEM image of the synthesized $Na_{2/3}Fe_{1/3}Mn_{2/3}O_2$ powders.

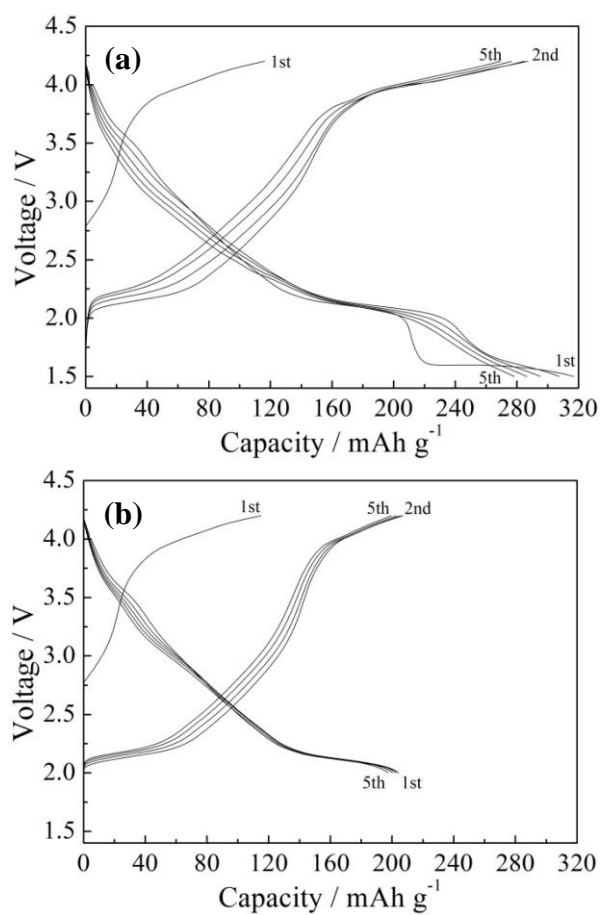**Figure 2.** Charge-discharge curves of the $Na_{2/3}Fe_{1/3}Mn_{2/3}O_2$ positive electrode at a current rate

of 20 mA g^{-1} and cut-off voltages of (a) 1.5–4.2 V and (b) 2.0–4.2 V

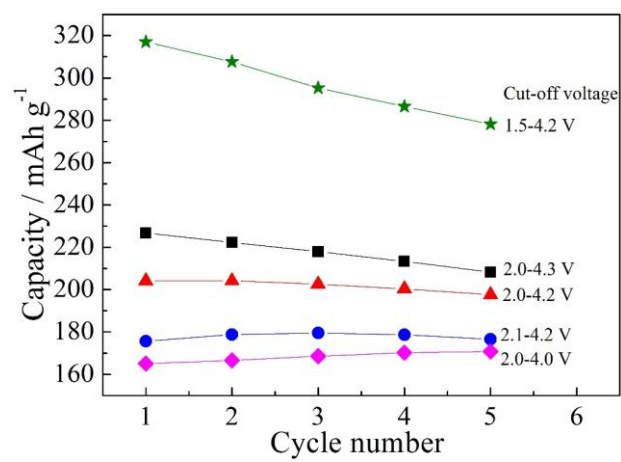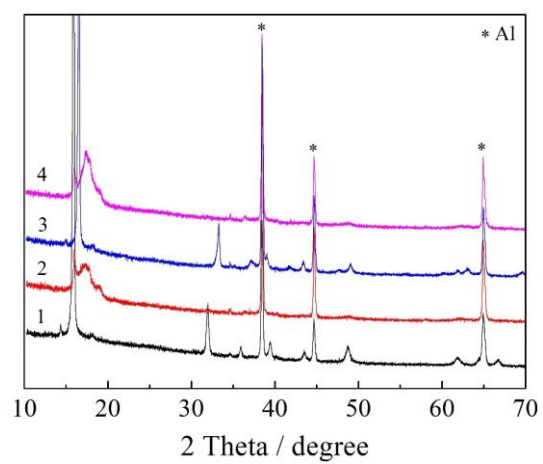**Figure 3.** Discharge capacity of the $Na_{2/3}Fe_{1/3}Mn_{2/3}O_2$ positive electrode at different cut-off voltages for current rate of 20 mA g^{-1}.

Figure 4. XRD patterns of the $Na_{2/3}Fe_{1/3}Mn_{2/3}O_2$ positive electrodes at different charge-discharge states: (1) before cycle; (2) charge to 4.2 V; (3) discharge to 2.0 V; and (4) recharge to 4.2 V.
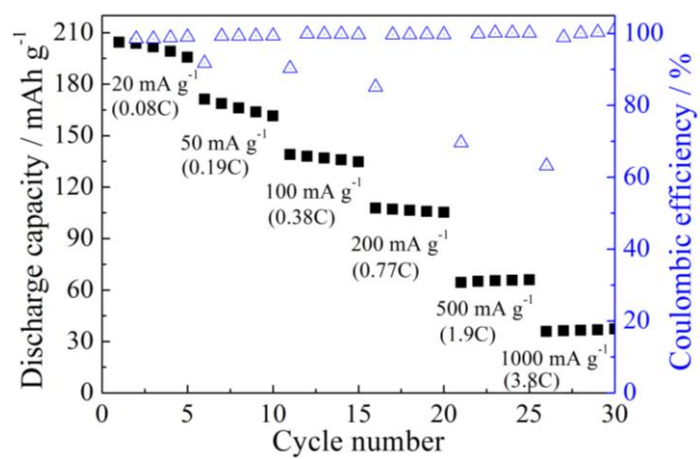
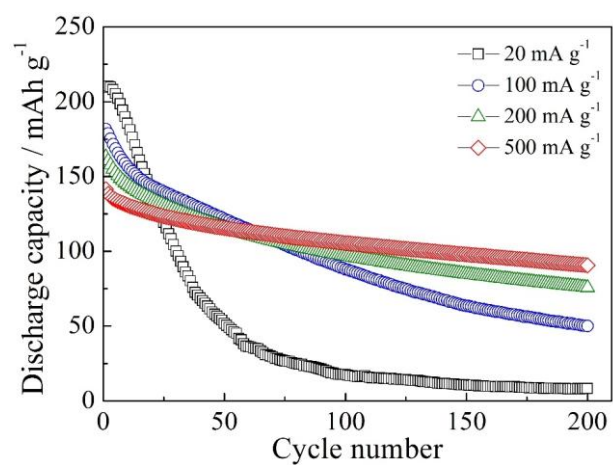**Figure 5.** Rate capability of the $Na_{2/3}Fe_{1/3}Mn_{2/3}O_2$ positive electrode in the voltage range of 2.0–4.2 V.

Figure 6. Cycle performance of the $Na_{2/3}Fe_{1/3}Mn_{2/3}O_2$ positive electrode at current rates of 20–500 mA g^{-1} in the voltage range of 2.0–4.2 V.